Multiphysics Analysis of Hemispherical Bulk Conductor Hertzian Contact Under Uniaxial Mechanical Load

Blaise Ravelo, Nicolas Peyret, Olivia Penas, Tanguy Davin

Multiphysics Analysis of Hemispherical Bulk Conductor Hertzian Contact Under Uniaxial Mechanical Load

Blaise Ravelo, *Member, IEEE*, Nicolas Peyret, Olivia Penas, and Tanguy Davin

***Abstract*—A multiphysics model of smoothed contact surface hemispherical contact under dynamic vibration stress is treated in this paper. The contact structure is applied to hemispherical conductor bulk materials. The structure electrothermomechanical (ETM) behavior is investigated based on the Hertz contact theory coupled with electrokinetic approach. An electrical circuit integrating the contact material properties is proposed. The contact surface deformation ETM expression is formulated. The transient variations of the contact conductor material temperatures in function of the mechanical vibrations are analytically described. The ETM parameters range versus the mechanical load stress is analyzed by considering aluminum alloy material hemispherical bulk with a radius varying from 10 μm to 1 mm. The contact radius can be totally deformed when the load is increased up to 20 kN. In addition, an innovative multiphysics computational method is validated numerically to determine the transient variation of the contact surface radius model from SPICE simulation by considering 0.5 kHz/1 kHz frequency presenting 0.5-kN amplitude sine wave, and arbitrary waveform dynamic vibrations. It was conjectured from numerical application, the hemispherical bulk contact temperature, and also the mechanism multiphysics phenomena governing the structure behavior. As ongoing research, the equivalent system tensorial statement illustrating the multiphysics interaction between the conductor contacts will be developed.**

***Index Terms*—Dynamic vibration, electrical contact, electrothermomechanical (ETM) behavior, mechanical contact, mechanical stress, multiphysics modeling, structural analysis.**

I. Introduction

THE connectors constitute one of the key elements constituting the electrical and electronic systems [1]. Therefore, the connector reliability plays an important role on the performance of electrical systems [2]. Fault analysis and diagnosis [3] are required in order to predict the behavior of the connectors against the different undesirable perturbations susceptible to affect the large electrical systems. To realize this behavioral analysis, the contact resistance is the main and basic parameter. It allows us to numerically and experimentally assess the connector performance and failure [4]. Electrical contact wire terminations standard has been met to ensure the specifications and quality [5]. Moreover, experimental and numerical investigations have been performed to study the mechanical vibration effects onto the connector elements [6]–[10]. Experimental tests showed that vibration stress induces spontaneous changes on the contact resistance of high-power electrical connectors for hybrid vehicles [7], [8].

In certain critical electrical environments, it was reported that the connectors can be damaged by the vibration stresses [9]. The material behavior constitutes one of the fundamental aspects during the analysis of the mechanical stressed connectors. It was assessed that mechanical vibrations can degrade gold- and copper-based contact materials [10]–[12]. The analysis of vibration stresses can be conducted with the influence of the slip amplitude and sliding effects [13], [14]. The sliding electrical contact affects the performance of high-speed connector data [14]. More recently, electromechanical multiphysics modeling of pin-socket structure under uniaxial vibration is proposed [15], [16]. Indeed, for the further understanding of the influence of vibration, electrothermomechanical (ETM) or multiphysics analysis can be necessary.

Few research works [17] are available for the typically third order of complexity multiphysics analysis with coupled electrical and mechanical and thermal phenomena. However, most of the studies available in the literature are either focused on electromechanical [6]–[16] or electrothermal [17]–[19] or thermomechanical [20]–[23] approaches. During the sliding motion, the contact resistance temperature is rising spontaneously [17]. Under high mechanical loads, the temperature elevation can change significantly the contact resistance [18]. Optimization techniques have been proposed in order to take into account the sliding contact resistance temperature [19]. Thermomechanical effects from sliding motion are generally investigated based on the tribology [22], [23]. So far, most of the contact resistance analyses are based on the Holm model [25]–[28]. Constriction resistance must be considered when the contact surface roughness is significant [25]–[27]. Numerical studies can also be performed in function of the contact geometry complexity [29]. But numerical approaches are generally not enough for the deep understanding on the ETM multiphysics analysis of the contact resistance.

This work was supported by the Carnot ESP 3 Program funded by the research project "Vibrations, Temperature and High Voltage Analysis for Connectors," 2017–2018. *(Corresponding author: Blaise Ravelo.)*

B. Ravelo is with the Normandy University UNIROUEN, Rouen F-76000, France (e-mail: blaise.ravelo@yahoo.fr).

N. Peyret and O. Penas are with the Laboratoire-QUARTZ, Saint Ouen F-93400, France (e-mail: nicolas.peyret@supmeca.fr; olivia.penas@supmeca.fr).

T. Davin is with the Centre Essais Vibro Acoustique Automobile, Saint Etienne du Rouvray F-76800, France (e-mail: t.davin@6-napse.com).

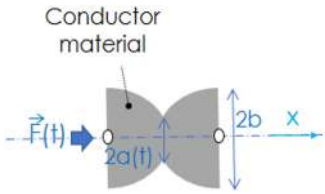

Fig. 1. Geometry of conductor contact material stressed by uniaxial load.

For this reason, this paper is focused on the multiphysics fast analysis of elementary spherical structure. The analysis is performed in function of both the uniaxial vibration load intensity and the voltage power supply amplitude. As a result, simple hemispherical metallic structure based on the sphere–sphere contact is analyzed based on the Hertzian elastic contact theory [30], [31]. The main aim of the study is to propose a multiphysics approach enabling to calculate the electrical parameter variation in function of the vibration stress amplitude. The surface roughness and the constriction resistance are not considered in this study. This paper is organized in three main sections. Section II describes the theoretical approach about the proposed multiphysics analysis. Section III addresses the numerical applications. At last, Section IV concludes this paper.

II. Description of the Elastic Hemispherical Conductors Under Uniaxial Mechanical Load

This section is dedicated to the analytical investigation of the multiphysics modeling concept applied to two spherical conductor contacts. It is worth noting that this study is limited to the ideal case of smooth surface contact. In other words, the effects of surface corrosion, wear, and fretting motion are neglected. As a complementary hypothesis, the considered contact problem is limited to the case of structure operating with a mechanical effort under static regime. Therefore, the transient behavior does not concern the concerned three ETM physics responses.

A. Hertzian Contact Structure Problem Formulation

For the best illustration of the developed theory, elastic hemispherical conductor materials are assumed as the structure under study. Fig. 1 illustrates the structure of the spherical conductor material contact. The contact area is localized between the metallic conductor interfaces. The interface contact is assumed pressed by a normal load $\overrightarrow{F}$. The Hertzian contact assumes the following.

1) The strains are small and within the elastic limit.
2) The surfaces are continuous and non-conforming.
3) The two bulk materials in contact can be considered as an elastic half-space.

As shown in Fig. 1, the contact object is constituted by two identical bulk materials. It is composed of two hemispherical parts with a radius denoted *b*. Let us denote the parameters of the two solids in contact as follows:

1) *E*1 and *E*2 are the Young moduli.
2) ν_1^2 and ν_2^2 the squares of the Poisson ratios.
3) *r*1 and *r*2 represent the bending radii of the two surfaces in contact.

According to the Hertz theory [34], which is more recently synthesized in [35], the contact area radius is defined as

$$a = (0.75 F a_0 / E^*)^{1/3} \tag{1}$$

where

$$1/E^* = (1-\nu_1^2)/E_1 + (1-\nu_2^2)/E_2 \tag{2}$$

and the generalized bending radius is given by

$$1/a_0 = 1/r_1 + 1/r_2. \tag{3}$$

By considering that the contact area is much smaller than lateral surfaces of solids in contact, the bending radii are known at the contact point, the solid are elastic, homogeneous, and isotropic, the contact is realized, without friction, and there is no relative motion between the two solids. For two solids presenting the same bending radii *b* and the same materials properties (*E* and *v*), the radius of the contact area expression becomes [1]

$$a = \left[0.75\left(1-\nu^2\right) F\, b/E\right]^{1/3}. \tag{4}$$

This configuration enables to describe the analytical formulation of the bulk material deformation in function of the uniaxial vibration stress parameters. To this end, the main variables are the vibration load action and the geometrical deformation. The structure is stressed by a time-dependent mechanical vibration normal load

$$\overrightarrow{F}(t) = F(t)\overrightarrow{e_z}. \tag{5}$$

This load is applied in the direction of the revolution axis $\overrightarrow{e_z}$ of the bulk material. Based on the Hertz contact theory, the contact surfaces can be assumed as circular with a time-dependent radius and the contact radius and the uniaxial load are linked by the relation [1]

$$F(t) = 4Ea^3(t)/\left[3b(1-\nu^2)\right]. \tag{6}$$

This equation enables to determine the mechanical load corresponding the surface contact deformation. However, the computation of the vibration load and the contact surface radius remains a challenging task.

B. Electrical Characterization Approach

The present electrical approach consists in analyzing the electrical current and voltage across the contact elements. Fig. 2 depicts the considered electrical schematic. This circuit is fed by a time-dependent voltage source *U*(*t*) placed between M_0 and M_1, as shown in Fig. 2(a). The electrical current can be obtained with the voltage across the resistive load R_0, which is placed between M_0 and M_1. The electrical equivalent scheme is established in Fig. 2(b). The partial resistance *R(t)* represents the time-dependent resistance between the bulk conductor section planes M_1M_2. The current flowing across the conductor can be extracted from different electrical laws. First, based on Ohm's law, we have

$$U = [R_0 + R(t)]\, I(t). \tag{7}$$

By inverting this relation, the current flowing across the conductor can be extracted. Second, by applying the voltage division

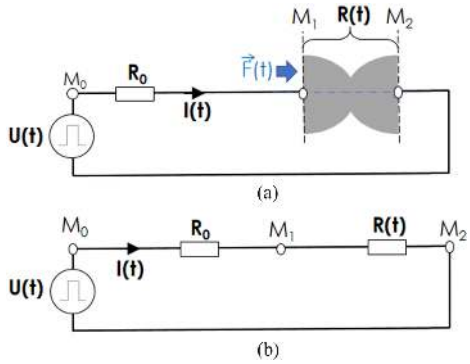

Fig. 2. (a) Diagram of the contact structure fed by the voltage source *U*(*t*) and (b) its equivalent schema.

principle, we have the voltage across the bulk materials

$$U_c(t) = V_{M_1M_2}(t) = U(t)R(t)/\left[R_0 + R(t)\right]. \tag{8}$$

The multiphysics model is investigated by extracting the mechanical and thermal variables from the electrical parameters. Based on the multiphysics phenomenon interactions around the contact interface, the mechanical deformation, electrical behavior, and thermal phenomena transform are expressed in the next section.

C. Mechanical Characterization From Electrical Parameters

By hypothesis, the bulk contact material has an electrical resistivity ρ. Based on the electrokinetic theory, the cylindrical slice with radius *x*(*t*) and height *dy* presents the differential resistance

$$dR(t) = \rho\, dy/\left[\pi x^2(t)\right]. \tag{9}$$

The time-dependent electrical equivalent resistance between the nodes M_1M_2 is calculated from the integration of the quantity by varying *x* from *a* to *b*

$$R(t) = 2\int_{a(t)}^{b} dR(t) = \rho/(2\pi b)\ln\left\{\left[b + a(t)\right]/\left[b - a(t)\right]\right\}. \tag{10}$$

The contact surfaces can be assumed as circular with a time-dependent radius introduced in (4). Substituting this expression into (9) yields the following relation:

$$R(t) = \frac{\rho}{2\pi b}\ln\left\{\frac{b + \left[3bF(t)(1-\nu^2)/(4E)\right]^{1/3}}{b - \left[3bF(t)(1-\nu^2)/(4E)\right]^{1/3}}\right\}. \tag{11}$$

Knowing the voltage across the contact bulk material, the deformation radius can be extracted from the following expression:

$$a(t) = b\left\{\frac{\exp\left[2\pi bR_0U_c(t)/\left[\rho(U(t) - U_c(t))\right]\right] - 1}{\exp\left[2\pi bR_0U_c(t)/\left[\rho(U(t) - U_c(t))\right]\right] + 1}\right\}. \tag{12}$$

D. Electrothermal Analysis

The overall system behavior can be investigated from this expression. The bulk material thermal heat is linked to the instantaneous electrical power. It is worth noting that the voltage drop across the contact U_c depends on the bulk contact temperature T_m defined by the Kohlrausch equation [27]

$$U_c^2 = 8\int_{T}^{T_m} \lambda(x)\rho(x)dx \tag{13}$$

with *T* is the bulk conductor temperature, T_m is the temperature at the contact point between the two bulk conductors, and λ is the thermal conductivity of the contact materials. The electrical and thermal conductivities of the bulk material in function of the environment temperature can be approximately expressed by the following linear relations, respectively:

$$\rho(T) \approx \rho_0(1 + a_\rho T) \tag{14}$$

$$\lambda(T) \approx \lambda_0(1 + a_\lambda T) \tag{15}$$

where $\rho_0 = \rho(T = T_0)$ is the electrical resistivity and a_ρ is the electrical resistivity thermal expansion coefficient, and $\lambda_0 = \lambda(T = T_0)$ is the thermal conductivity at $T = T_0$ and a_λ is the thermal conductivity thermal expansion coefficient. The thermal expansion coefficients of the electrical resistivity and the thermal conductivity are, respectively, denoted a_ρ and a_λ. Knowing the bulk resistance at the reference temperature T_0, the bulk resistance can also be expressed with the linear relation:

$$R(T) \approx R(T_0)\left[1 + a_\rho(T - T_0)\right]. \tag{16}$$

E. ETM Analysis

The developed multiphysics analysis can be deduced by combining the different previous expressions. The electrical, mechanical, and thermal physics effects can be explored by taking into account the analytical definition of the resistance previously defined in (10) and thermal linear expansion relations in (14)–(16). Emphatically, the propagating current *I* can be expressed from Ohm's law

$$I = U/\left[R_0 + R_b(1 + a_\rho T)\right] \tag{17}$$

where the resistance R_b in function of the ETM parameters is deduced from (11) $R_b = R(t)$. Moreover, substituting (13) into (14) yields the relation

$$U^2R^2 - 8(R + R_0)^2\int_{T}^{T_m} \rho(x)\lambda(x)dx = 0. \tag{18}$$

The contact temperature and the current propagating through the bulk can be extracted from this equation. Let us consider three different cases in function of the temperature dependence of the electrical resistivity and thermal conductivity. Thereby, depending on the considered complexity, fundamental equation (18) can be modified, as expressed in the next paragraphs.

1) Case 1: In this case, we assume that

$$\begin{cases} \rho(T) \approx \rho_0 = C^{te} \\ \lambda(T) \approx \lambda_0 = C^{te} \end{cases}. \tag{19}$$

Then, we can suppose also that $R = R_b$. The contact temperature yielded from (18), which is merely reduced to first degree equation, can be approximately expressed as

$$T_m^{(1)} = U^2R^2/\left[8\rho_0\lambda_0(R + R_0)^2\right] + T. \tag{20}$$

The relative difference with the ambient temperature is given by

$$\Delta T^{(1)} = U^2 R^2 / \left[8\rho_0\lambda_0(R+R_0)^2\right]. \tag{21}$$

The difference between the approximated contact and the environment absolute temperature does not depend on the environment temperature.

2) Case 2: The present case is defined with the particular parameters

$$\begin{cases} \lambda(T) \approx \lambda_0 = C^{te} \\ \rho(T) \approx \rho_0(1+a_\rho T) \end{cases}. \tag{22}$$

It implies the modification of (18) in function of the bulk and contact temperatures that can be rewritten with the vibration load and the temperature parameters. The fundamental equation of the bulk material contact temperature can be written as a second-order polynomial equation

$$c_2(T)(T_m^{(2)})^2 + c_1(T)T_m^{(2)} + c_0(T) = 0 \tag{23}$$

where

$$\begin{cases} c_2(T) = -4\rho_0\lambda_0 a_\rho[R_0 + R_b(1+a_\rho T)]^2 \\ c_1(T) = -8\rho_0\lambda_0[R_0 + R_b(1+a_\rho T)]^2 \\ c_0(T) = c_{04}T^4 + c_{03}T^3 + c_{02}T^2 + c_{01}T + c_{00} \end{cases} \tag{24}$$

and

$$\begin{cases} c_{04} = 4\rho_0\lambda_0 a_\rho^3 R_b^2 \\ c_{03} = 8\rho_0\lambda_0 a_\rho^2 R_b(R_0+2R_b) \\ c_{02} = a_\rho\left[4\rho_0\lambda_0(R_0+R_b)(R_0+5R_b) + a_\rho R_b^2 U^2\right] \\ c_{01} = 2\left[4\rho_0\lambda_0(R_0+R_b)^2 + a_\rho R_b^2 U^2\right] \\ c_{00} = R_b^2 U^2 \end{cases}. \tag{25}$$

3) Case 3: In this last case, the electrical and thermal conductivities are temperature dependent

$$\begin{cases} \rho(T) \approx \rho_0(1+a_\rho T) \\ \lambda(T) \approx \lambda_0(1+a_\lambda T) \end{cases}. \tag{26}$$

In this case, (14) is transformed as a third-degree polynomial equation

$$c_3(T)(T_m^{(3)})^3 + c_2(T)(T_m^{(3)})^2 + c_1(T)T_m^{(3)} + c_0(T) = 0 \tag{27}$$

where

$$\begin{cases} c_3(T) = 8\rho_0\lambda_0 a_\rho a_\lambda[R_0 + R_b(1+a_\rho T)]^2/3 \\ c_2(T) = 4\rho_0\lambda_0(a_\lambda - a_\rho)[R_0 + R_b(1+a_\rho T)]^2 \\ c_1(T) = -8\rho_0\lambda_0[R_0 + R_b(1+a_\rho T)]^2 \\ c_0(T) = c_{05}T^5 + c_{04}T^4 + c_{03}T^3 + c_{02}T^2 + c_{01}T + c_{00} \end{cases} \tag{28}$$

TABLE I
CONDUCTOR AA-1350 ALUMINUM MATERIAL PROPERTIES

Properties	Value
Young's modulus	62 GPa
Poisson's ratio	0.24
Electrical resistivity @ 20°C	25.6 nΩ.m
Temperature coefficient electrical resistance	4.24×10^{-3}/°C
Thermal conductivity @ 20°C	243 W/m/°C
Thermal conductivity expansion	271×10^{-6}/°C
Specific heat capacity	900 J/kg/K
Density	2700 kg/m^3

TABLE II
GEOMETRICAL PARAMETERS

Parameter	Range of values
Radius b	10 µm to 1 mm
Radius a	b/10 to b

and

$$\begin{cases} c_{05} = -8\rho_0\lambda_0 a_\rho^3 a_\lambda R_b^2/3 \\ c_{04} = 4\rho_0\lambda_0 a_\rho^2 R_b\left[3a_\rho R_b - a_\lambda(4R_0+7R_b)\right]/3 \\ c_{03} = 8\rho_0\lambda_0 a_\rho \begin{bmatrix} a_\lambda(R_0+R_b)(R_0+4R_b) \\ -3a_\rho R_b(R_0+2R_b) \end{bmatrix} \Big/ 3 \\ c_{02} = a_\rho^2 R_b^2 U^2 + \rho_0\lambda_0 \begin{bmatrix} 4a_\rho(R_0+R_b)(R_0+5R_b) \\ -4a_\lambda(R_0+R_b)^2 \end{bmatrix} \\ c_{01} = 2\left[4\rho_0\lambda_0(R_0+R_b)^2 + a_\rho R_b^2 U^2\right] \\ c_{00} = R_b^2 U^2 \end{cases}. \tag{29}$$

The solutions of those equations enable to approximate the contact temperature and also the current propagating through the bulk materials. Applications examples with contact structure under vibration load are examined in the next section.

III. ILLUSTRATIVE APPLICATION EXAMPLE

The present section introduces an illustrative numerical application of the previously established modeling approach. The relevance of the developed multiphysics theory is checked with an application example of metallic contact. After the description of the test contact structure parameter, the calculated results will be presented. Then, the graph formulation of the proposed model will be drawn.

A. Analysis Structure Parameters

As an arbitrary example of test material structure, the Aluminum material AA-1350 is considered for the proposal numerical application. The different properties necessary for elaborating the contact structure model are summarized in Table I. The calculations of the contact resistance in function of the mechanical load are performed based on these properties. Then, the geometrical parameter ranges of values are addressed in Table II.

Before the numerical applications, we would like to remind that the Hertz contact assumptions enable to define the validity domain of the analytical model versus FEM simulation. For the

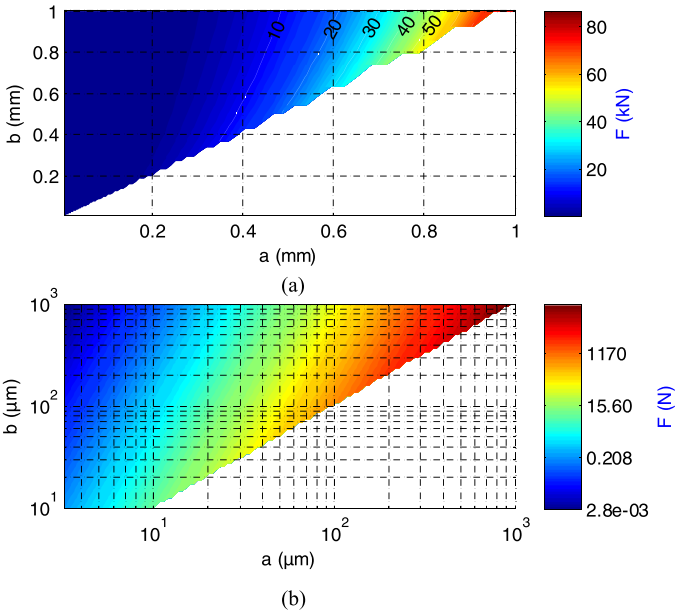

Fig. 3. Mechanical load intensity versus the geometrical parameters a and b.

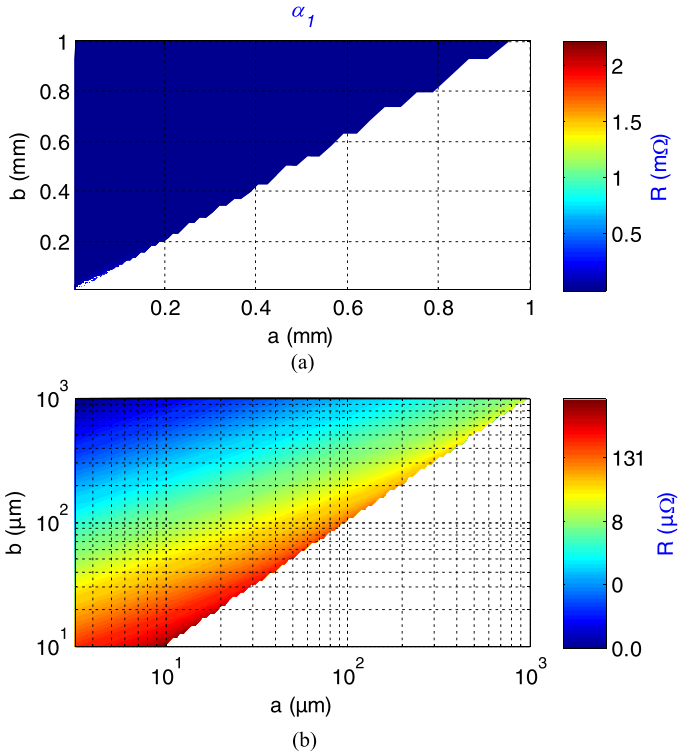

Fig. 4. Considered bulk contact conductor contact resistance versus the geometrical parameters a and b.

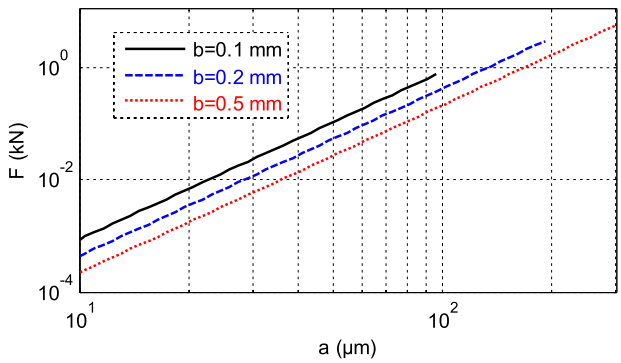

Fig. 5. Mechanical load intensity versus a for $b = \{0.1\text{ mm}, 0.2\text{ mm}, 0.5\text{ mm}\}$.

interaction property, a hard contact for the normal behavior and a frictionless for the tangential one has been chosen. Furthermore, other configurations for tangential behavior have been tested as penalty, static-kinetic exponential decay, rough, and Lagrange multiplier. The following section describes the analytically calculated results.

B. Application Results

This numerical investigation could be useful to analyze the material behaviors for the bulk conductor structure under mechanical stress. Static and dynamic mechanical stresses can be considered given a range of the mechanical amplitude. Particular use case as mechanical vibration can be considered.

1) Mechanical Load Effect Investigation: Based on formula (7), the cartographies of the mechanical load and contact resistance corresponding to the contact material surface deformation in function of the geometrical parameters are explored in this paragraph. For each value of the spherical material radius b, the mechanical load has been calculated for a varied from $b/10$ to b.

Fig. 3(a) and (b) shows the calculated map of the load intensity versus (a,b), respectively, represented in linear and logarithmic scales. The contact load can increase up to 80 kN to reach the contact radius variation up to 0.9 mm. Similar calculated results of the contact resistance cartographies in linear and logarithmic scales are, respectively, revealed in Fig. 4(a) and (b). The contact resistance can increase up to some milli-Ohms. These numerical results highlight the bulk material behavior through the contact radius variation. As illustrated by the curves plotted in Fig. 5, it can be concluded that the following statements hold.

1) For $b = 0.1$ mm, when F varies from about 1 to 783 N, the contact radius a varies from 1 to 96 μm.
2) For $b = 0.2$ mm, when F varies from about 0.4 N to 3.06 kN, the contact radius a varies from 1 to 191 μm.
3) For $b = 0.5$ mm, when F varies from about 0.2 N to 5.09 kN, the contact radius a varies from 1 to 285 μm.

2) FEM Validation of the Mechanical Model: The three-dimensional (3-D) design of the mechanical structure introduced in Fig. 6(a) was simulated with the commercial tool Abaqus in order to validate the analytical model of the contact area radius. By considering the mechanical normal load varying from 0 to 3 kN, we obtain the calculated and finite-element method (FEM) based simulation comparative results plotted in Fig. 6(b). It can be seen that a very good correlation of the contact surface radius is obtained with an absolute error less than 20 μm.

3) SPICE Validation of the Electromechanical Model: SPICE simulations were realized in order to validate the prediction of the deformed contact radius versus the dynamic vibration stress. Fig. 7 illustrates the schematic of the transient

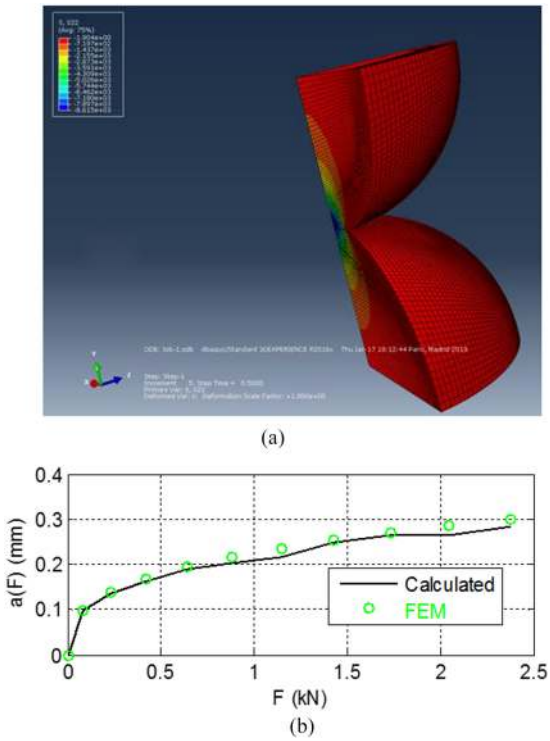

Fig. 6. (a) Abaqus 3-D design and (b) comparison between the proposed and FEM-computed contact surface radius.

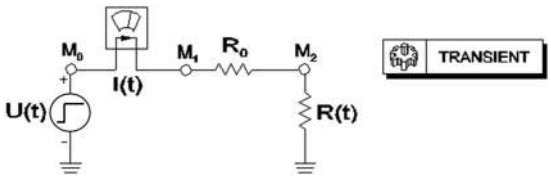

Fig. 7. SPICE schematic of the simulated circuit.

simulated circuit. It is fed by a unit step voltage with amplitude $U = 1$ V with an internal resistance $R_0 = 0.1\ \Omega$. The resistance $R(t)$ integrates the effect of three different dynamic vibration signals $F_1(t)$, $F_2(t)$, and $F_3(t)$ plotted in Fig. 8. The sine wave signals $F_1(t)$ and $F_2(t)$ present 0.5-kN amplitude and frequencies 0.5 and 1 kHz, respectively. $F_3(t)$ is an arbitrary waveshape varying from 0 to 1 kN. These slow-wave dynamic signals are considered in the time window of 10-ms duration and 0.1-ms step sampling. The simulated transient plots of the voltage U_c across the bulk material are shown in Fig. 9. The voltages fluctuate between 0 to 20 μV with a frequency two times less than the vibration load one. The comparisons between the direct calculated and extracted contact surface radius from U_c are presented in Fig. 10. A very good correlation is found at the different instantaneous time. The contact surface radius a varies from 0 to 250 μm for the cases of sine-wave vibration stress. However, a fluctuates between about 55 and 230 μm for the case of an arbitrary waveform vibration stress.

4) Investigation on the Environment Temperature and Mechanical Load Combined Effect: To investigate the ETM behavior, the structure was assumed fed by dc voltage source $U = 1$ kV and internal resistance $R_0 = 10\ \Omega$. The considered environment

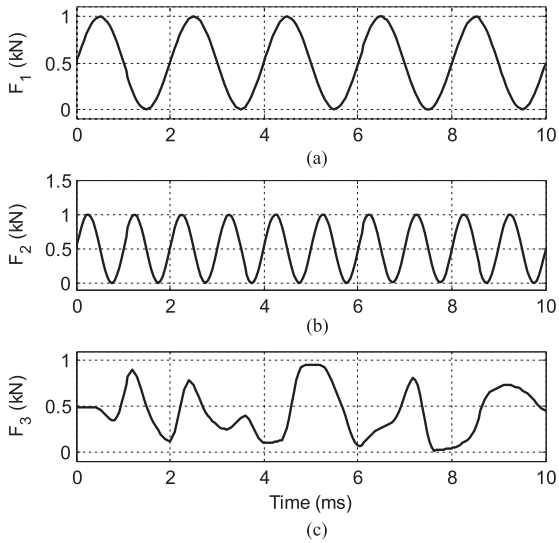

Fig. 8. Plots of the time-dependent vibration loads.

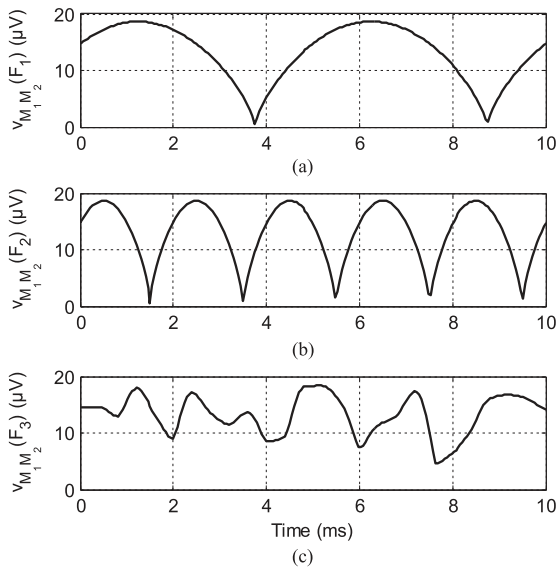

Fig. 9. Transient plots of voltage across the bulk materials.

temperature T varies from 20 to 100 °C. The mechanical load F is assumed to vary from 1 to 10 kN. The approximative contact temperatures $T_m^{(1)}$, $T_m^{(2)}$, and $T_m^{(3)}$ are calculated based on the equations proposed in previous sections (Sections II-D1–II-D3). The absolute difference between the contact and environment temperatures versus (F,T) is displayed in Fig. 11. For case 1, as highlighted by Fig. 11(a), the temperature difference varies from about 0.6 °C for the load 10 kN to about 1.1 °C for the load 1 kN independently to the environment temperature. As shown in Fig. 11(b) and (c), for the approximated cases 2 and 3, the absolute temperature difference increases with the environment temperature. Fig. 12 shows the absolute differences between the assessed contact temperatures for the proposed three different cases. The difference between case 1 and case 2 or 3 at high environment temperature can increase up to 0.4 °C.

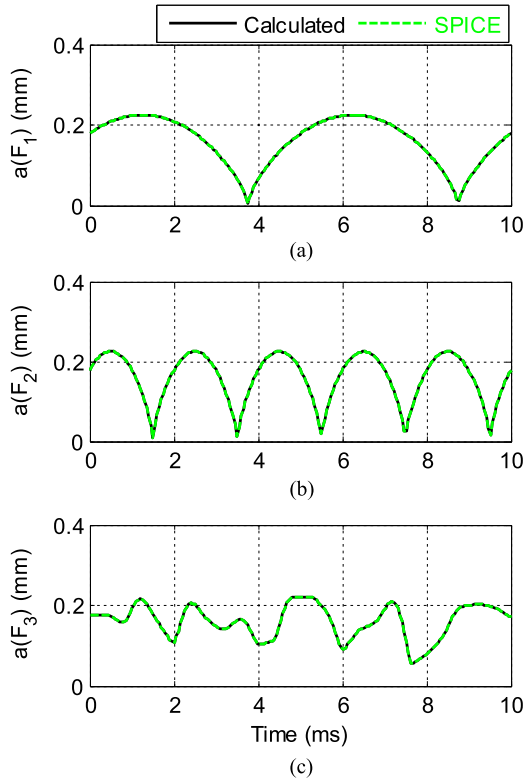

Fig. 10. Comparison of transient plots of SPICE simulated and calculated deformation from the multiphysics model.

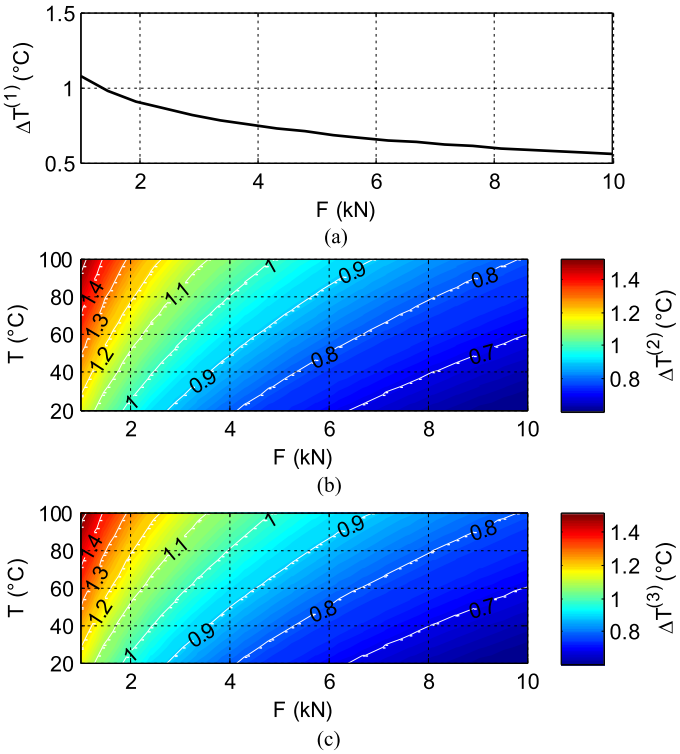

Fig. 11. Absolute difference between the contact temperatures: (a) $\Delta T^{(1)} = |T_m^{(1)} – T|$. (b) $\Delta T^{(2)} = |T_m^{(2)} – T|$. (c) $\Delta T^{(3)} = |T_m^{(3)} – T|$ versus (F, T).

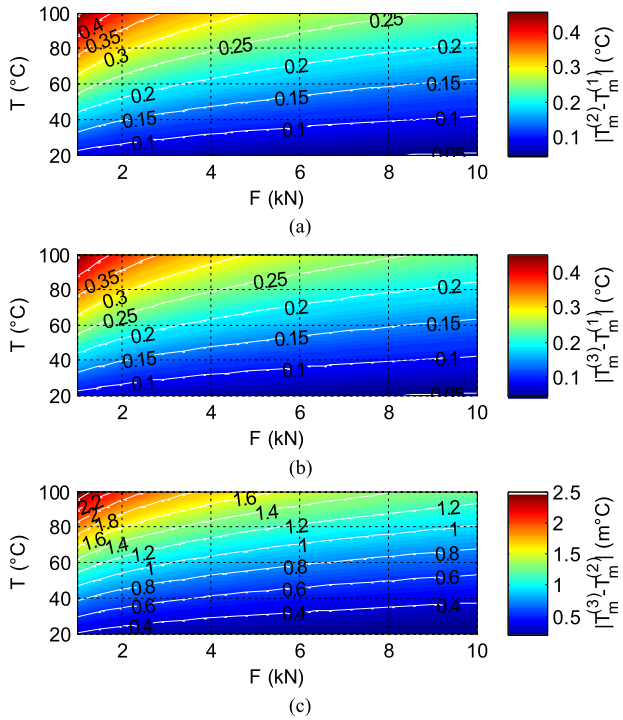

Fig. 12. Absolute difference between the contact temperatures (a) $|T_m^{(2)} – T_m^{(1)}|$. (b) $|T_m^{(3)} – T_m^{(1)}|$. (c) $|T_m^{(3)} – T_m^{(2)}|$ versus (F, T).

However, the difference is only of about some milli-degree Celsius between cases 2 and 3. This numerical application illustrates that the electrical thermal expansion effect dominates the thermal expansion for the considered material. Fig. 13 states about the propagating current absolute differences between the considered three different cases. Compared with case 1, the difference can reach 5 μA at high environment temperature. The difference between cases 2 and 3 is approximately some nanoseconds.

It is noteworthy that with the considered proof-of-concept structure, under normal load range up 2.4 kN, the thermal expansion generates 21-μm sphere radius variation. The 80 °C thermal variation induces 0.7% contact radius relative increase.

C. Advantages and Drawbacks of the Proposed Multiphysics Model

Compared to the 3-D meshing recursive computational based algorithm, the multiphysics model presents the following.

1) Advantages
   a) The possibility to simultaneously integrate the electrical, mechanical, and thermal phenomenologies. The proposed model indeed succeeds in taking into account the ETM effects.
   b) The flexibility of the analytical implementation with the consideration of different physical parameters, as the contact degradation mechanism by the corrosion and wear effects which could be added.
   c) The computational speed of the order of a millisecond for one configuration.

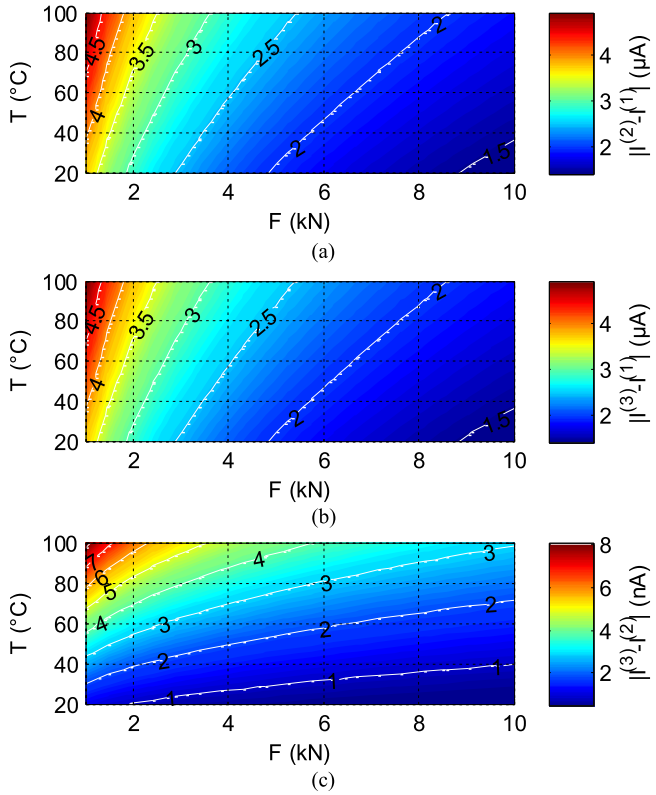

Fig. 13. Absolute difference between the currents (a) $|I^{(2)}–I^{(1)}|$, (b) $|I^{(3)}–I^{(1)}|$, and (c) $|I^{(3)}–I^{(2)}|$ versus (F, T).

2) And the main drawback is the difficulty to consider the inhomogeneity and anisotropy of the bulk material. Indeed, the analytical expressions could be more complicated and less accurate if the material parameters are not uniform. More generally, the proposed model is defined on the direct substitutions between the physical laws, using a so-called weak coupling. In prospects, it would be interesting to investigate on a formulation of an ETM model, going on a higher level of representation, reinforcing the coupling between the different physics.

IV. Conclusion

A multiphysics modeling of a metallic hemispherical contact with ideal smooth contact is developed. The material structure consists of conductor electrical contact under uniaxial vibration stress. The theoretical approach illustrates the mechanism of coupled thermal, mechanical, and electrical phenomena. The analytical approach corresponding to the multiphysics model of the structure is elaborated. The developed model combines the electrical aspect based on the classical circuit theory and the mechanical aspect based on the Hertzian contact theory. The transient behavior of the bulk material contact surface in function of the vibration stress is expressed.

Three phases of numerical applications are presented to illustrate the relevance of the proposed multiphysics model. First, the mechanical sensitivity of the structure in function of the stress load is discussed. Then, it shows that the multiphysics model is validated with a SPICE simulation showing contact surface transient variation in function of the sine wave (with amplitude 0.5 kN and 0.5 kHz/1 kHz frequencies) and arbitrary waveform dynamic vibration stresses (varying from 0 to 1 kN). It is shown how to predict the magnitude of the current propagating through the contact materials. Finally, the prediction of the contact temperature in function of the electrical and mechanical stresses in the hemispherical bulk contact is discussed. The Hertz model configurations allow us to consider same contact zone as in FEM simulation, but they allow a less computation time and a better precision for of the edge contact pressure evaluation.

As ongoing research, the coupled ETM model of contact structures taking into account the transient and multiscale time aspect is in progress. The ETM effects on the electronic and electrical component reliability is currently one of the unsolved and open problems in the different engineering areas such as power electronic, automotive, aeronautics, and aerospace. The proposed multiphysics model can be a pioneer work enabling to establish a prominent calculation for investigating the predictive reliability of electronic and electrical devices and notably through by their contacts with conductor materials.

Acknowledgement

The authors would like to thank Dr. O. Maurice from ARIANE GROUP, France, for his scientific help and encouragement to write this paper.

References

[1] J. R. S. Mroczkowski and J. M. Maynard, “Estimating the reliability of electrical connectors,” *IEEE Trans. Rel.*, vol. 40, no. 5, pp. 507–512, Dec. 1991.

[2] Y. V. Murty and G. K. Sujan, “Electrical and electronic connectors: Materials and technology,” *Mater. Sci. Mater. Eng.*, pp. 1–12, Mar. 2016.

[3] R. S. Mroczkowski, “A perspective on connector reliability,” in *Proc. 50th IEEE Holm Conf. Elect. Contacts/22nd Int. Conf. Elect. Contacts*, Seattle, WA, USA, Sep. 2004, pp. 1–28.

[4] R. Ji, J. Gao, G. Xie, and Q. Jin, “Fault analysis and diagnosis of coaxial connectors in RF circuits,” *IEICE Trans. Electron.*, vol. 100-C, no. 11, pp. 1052–1060, 2017.

[5] R. D. Malucci, “Stability and contact resistance failure criteria,” *IEEE Trans. Componen. Packag. Technol.*, vol. 29, no. 2, pp. 326–332, Jun. 2006.

[6] ASTM Committee B02, *Standard Guide for Specification and Quality Assurance for the Electrical Contact Performance of Crimped Wire Terminations*, Standard Document, B02.11 Elect. Contact Test Methods, B942-05, pp. 1–9, Dec. 2005.

[7] F. Zhang, “A study of vibration-induced fretting corrosion in electrical connectors based on experimental test and FEA simulation,” *M.Sc. thesis*, Auburn Univ., Auburn, AL, USA, 2014.

[8] R. Fu *et al.*, “Vibration-induced changes in the contact resistance of high power electrical connectors for hybrid vehicles,” *IEEE Trans. Compon. Packag. Technol.*, vol. 2, no. 2, pp. 185–193, Feb. 2012.

[9] R. Fu, S.-Y. Choe, R. L. Jackson, G. T. Flowers, and D. Kim, “Modeling and analysis of vibration-induced changes in connector resistance of high power electrical connectors for hybrid vehicles,” *Mech. Based Des. Struct. Mach.*, vol. 40, no. 3, pp. 349–365, 2012.

[10] T. Gissila, “Connectors and vibrations – damages in different electrical environments,” *M.Sc. thesis*, Blekinge Inst. Technol., Karlskrona, Sweden, 2013, pp. 1–112.

[11] W. Ren, L. Cui, J. Chen, X. Ma, and X. Zhang, “Fretting behavior of au plated copper contacts induced by high frequency vibration,” in *Proc. IEEE 58th Holm Conf. Elect. Contacts*, Portland, OR, USA, Sep. 2012, pp. 1–7.

[12] S. Ming, M. Pecht, and M. A. E. Natishan, "A comparative assessment of gold plating thickness required for stationary electrical contacts," *Microelectron. J.*, vol. 30, no. 3, pp. 217–222, 1999.

[13] G. Husheng, G. Haicheng, and Z. Huijiu, "Effect of slip amplitude on fretting fatigue," *Wear*, vol. 148, no. 1, pp. 15–23, Aug. 1991.

[14] G. F. Dorsey, D. S. Coleman, and B. K. Witherspoon, "High speed data across sliding electrical contacts," in *Proc. IEEE 58th Holm Conf. Elect. Contacts*, Portland, OR, USA, Sep. 2012, pp. 1–12.

[15] B. Ravelo, "Multiphysics analysis of pin-socket electrical dynamic contact susceptibility under vibration stress," *IEEE Trans. Electromag. Compat.*, vol. 61, no. 2, pp. 344–351, Apr. 2019.

[16] B. Ravelo, "Multiphysics TAN modelling of uniaxial vibration loaded pin-socket electrical contact," *IEEE J. Multiscale Multiphys. Comput. Techniq.*, vol. 3, no. 1, pp. 50–57, Dec. 2018.

[17] A. Monnier, B. Froidurot, C. Jarrige, R. Testé, and R. Meyer, "A mechanical, electrical, thermal coupled-field simulation of a sphere-plane electrical contact," *IEEE Trans. Componen. Packag. Technol.*, vol. 30, no. 4, pp. 787–795, Dec. 2007.

[18] E. Rabinowicz, "The temperature rise at sliding electrical contacts," *Wear*, vol. 78, no. 1–2, pp. 29–37, May 1982.

[19] M. Vogler and S. Sheppard, "Electrical contact resistance under high loads and elevated temperatures," *Welding Res. Suppl.*, vol. 72, pp. 231–238, Jun. 1993.

[20] R. El Abdi and N. Benjemaa, "Contact resistance and temperature optimizations for high copper alloys used in electrical contacts," in *Proc. 7th WSEAS Int. Conf. Appl. Elect. Eng.*, Trondheim, Norway, Jul. 2008, pp. 83–87.

[21] I. Petre, E. V. Stoian, and M. C. Enescu, "Determining the heat regime in the working of a coupling with sliding motion," *Sci. Bull. Valahia Univ. Mater. Mech.*, vol. 14, no. 11, pp. 33–38, 2016.

[22] E. Carvou, R. EI Abdi, J. Razafiarivelo, N. Benjemaa, and E. M. Zindine, "Thermo-mechanical study of a power connector," *Measurement*, vol. 45, no. 5, pp. 889–896, 2012.

[23] R. A. Burton, "Thermomechanical effects in sliding wear," Document AD-A055 318, N0001A-75-C-0761, Northwestern Univ., Evanston, IL, USA, 1978, pp. 1–34.

[24] J. Rivière, M. Renouf, and Y. Berthier, "Thermo-mechanical investigations of a tribological interface," *Tribol. Lett.*, vol. 58, no. 48, pp. 48–59, 2015.

[25] R. Prieto *et al.*, "Thermo-mechanical assessment of copper and graphite heat spreaders for compact packages," in *Proc. 22nd Int. Workshop Thermal Investigations ICs Syst.*, Budapest, Hungary, Sep. 2016, pp. 19–22.

[26] J. A. Greenwood, "Constriction resistance and the real area of contact," *Brit. J. Appl. Phys.*, vol. 17, pp. 1921–1932, Dec. 1966.

[27] D. Guha and S. K. Roy Chowdhuri, "The effect of surface roughness on the temperature at the contact between sliding bodies," *Wear*, Vol. 197, no. 1–2, pp. 63–73, Sep. 1996.

[28] M. D. Bryant, "Resistance buildup in electrical connectors due to fretting corrosion of rough surfaces," *IEEE Trans. Compon. Packag. Technol.*, vol. 17, no. 1, pp. 86–95, Mar. 1994.

[29] R. S. Timsit, "Electrical conduction through small contact spots," in *Proc. 50th IEEE Holm Conf. Elect. Contacts/22nd Int. Conf. Elect. Contacts*, Seattle, WA, USA, Sep. 2004, pp. 184–191.

[30] P. Lindholm, "Numerical study of coated electrical contacts," in *Proc. COMSOL Conf.*, Paris, France, 2010, pp. 1–6.

[31] Bryant, "Contact," Lecture note, 2006. [Online]. Available: http://www.me.utexas.edu/∼bryant/courses/me383s/DownloadFiles/LectureNotes/Contact.pdf

[32] S. J. Shaffer, "Tribology 101 – Introduction to the Basics of Tribology," BRUKER, 2017. [Online]. Available: https://www.bruker.com/fileadmin/user_upload/8-PDF-Docs/SurfaceAnalysis/TMT/Webinars/Tribology_101_Webinar-1_Intro_and_Basics_29-Jan-2013.pdf

[33] R. E. Bolz, *Handbook of Tables for Applied Engineering Science*. Boca Raton, FL, USA: CRC Press, 1973.

[34] H. Hertz, "On the contact of elastic solids," *J. fur die Reine und Andgewandte Mathematik*, vol. 92, no. 110, pp. 156–171, 1882.

[35] K. Johnson, *Contact Mechanics*. Cambridge, U.K.: Cambridge Univ. Press, 1987.